Journal of Alloys and Compounds 797 (2019) 717–726

Contents lists available at ScienceDirect

Journal of Alloys and Compounds

journal homepage: http://www.elsevier.com/locate/jalcom

The influence of boron doping on the structural and mechanical characterization of ZnO

Sevim Demirozu Senol [a, *], Rıfkı Terzioglu [b], Ozgur Ozturk [c]

[a] Department of Chemistry, Bolu Abant Izzet Baysal University, 14280 Bolu, Turkey
[b] Department of Electrical and Electronics Engineering, Bolu Abant Izzet Baysal University, 14280 Bolu, Turkey
[c] Department of Electrical and Electronics Engineering, Kastamonu University, 37100 Kastamonu, Turkey

ARTICLE INFO

Article history:
Received 27 February 2019
Received in revised form
7 May 2019
Accepted 13 May 2019
Available online 16 May 2019

Keywords:
B-doped ZnO
Hydrothermal method
Vickers microhardness
HK approach

ABSTRACT

In this study, we have reported the structural and mechanical properties of B-doped ZnO ($Zn_{1-x}B_xO$, x = 0.00, 0.05, 0.07, 0.09, 0.11) by using XRD, SEM, EDS and static Vickers micro-hardness measurements. All nanopowder samples were prepared by hydrothermal method. From the XRD measurements, we have found that all the samples crystalize in hexagonal wurtzite structure and crystallite sizes were found to be 61.50, 36.97, 36.65, 36.59 and 34.85 nm for x = 0.00, 0.05, 0.07, 0.09, 0.11 samples, respectively. From the SEM measurements, the irregular appearance and size distribution of the particles were observed for all samples. The chemical composition of $Zn_{1-x}B_xO$ nanopowders were investigated by EDX spectroscopy. Zn,O and B peaks are clearly seen and the content of Zn, O and B are consistent with preparation of samples. From the load dependent indentation diagonal length measurements, load dependent (apparent) hardness, elastic modulus, yield strength, and fracture toughness values of the samples were computed. The hardness values increase with increasing the boron content and the applied load. In addition, the apparent hardness values were analyzed by using the various theoretical models to evaluate the load independent (true) hardness values. The IIC model was found to be sufficient for our investigations. The possible reasons for the observed changes in mechanical, structural properties due to B-doping in ZnO were discussed.

1. Introduction

ZnO is an important technological material because of its considerable performance in electronics, optics and photonics [1,2]. Since ZnO has strong piezoelectric and pyroelectric properties arising from the absence in its wurtzite structure with a hexagonal lattice, wide band gap (3.37eV) and large electrochemical coupling, it is widely used in piezoelectric sensors, mechanical actuators [3,4]. In addition, it has an extensive application in the photoelectrical devices, photovoltaic applications and solar cell heterojunction [5–8].

Morever, the mechanical properties of ZnO-based semiconductors such as hardness, elastic modulus, fracture toughness, brittleness and yield strength play an important role in production of optoelectronic devices. The variations in mechanical properties is directly related to interatomic bounding force of the materials. Therefore, one of the procedure used in the literature to increase the mechanical properties of ZnO-based semiconductor materials is to add different types of atoms into the ZnO structure [9–12].

It has been suggested that B doped ZnO might enhance its mechanical properties; for example, hardness of the undoped ZnO films is much lower than that of B-doped ZnO sample [13]. Although the study on properties of electrical, magnetic and optical of B-ZnO is intensively studied, the mechanical properties is rarely studied in the literature.

One of the most common used methods to determine the mechanical properties of materials is the Vickers hardness test. The method was developed as an alternative to the Brinell method in 1921 by British researchers Vickers, Smith and Sandland [14]. The system is based on the optical measurement of the 136° diamond pyramid tip, with specific loads selected depending on the material type and thickness. In addition, Vickers hardness is similar to the Brinell method because it is an optical hardness measurement method. Vickers hardness test can be performed for all specimens due to having the largest scales among the hardness measurements.

* Corresponding author.
E-mail address: demirozu_s@ibu.edu.tr (S.D. Senol).

https://doi.org/10.1016/j.jallcom.2019.05.140
0925-8388/

It is well known that the microhardness of the solids is load dependent. The microhardness decreases with increasing the applied test-load which is called the Indentation Size Effect (ISE) while it increases with the increase in the applied load which is named Reverse Indentation Size Effect (RISE) behavior [15]. The determination of these behaviors of materials is very important in terms of usage in technological applications.

The main objective of this study is to investigate the effect of boron concentration on the structural and mechanical properties of $Zn_{1-x}B_xO$ ($x = 0$, 0.05, 0.07, 0.09, 0.11) samples prepared by using the hydrothermal method. In this study, the mechanical properties of the samples were evaluated and the load dependent Vickers micro-hardness data were analyzed by using the most widely used methods in the literature such as Meyer's Law, the Proportional Sample Resistance, Elastic/Plastic Deformation, Indentation-Induced Cracking (IIC) and Hays-Kendall (HK) models. To the best of our knowledge, no detailed study on the effects of B addition on the structural and mechanical properties of ZnO has been published in the literature.

2. Experimental

$Zn_{1-x}B_xO$ were prepared as polycrystalline nanopowders with various compositions ($x = 0$, 0.05, 0.07,0.09,0.11) using hydrothermal method. In synthesis process, Zinc acetatedihydrate, ($Zn(CH_3COO)_2 2H_2O$) (Merck), hexamethylenetetramine, (HMT) (Merck), were mixed thoroughly in an appropriate proportion and dissolved in deionized (DI) water to obtain equimolar aqueous solution. Then, boric acid, (H_3BO_3) Merck, was added with different concentrations ($x = 0.0$, 0.05, 0.07, 0.09, 0.11) and was stirred using the magnetic stirrer at room temperature for 2 h until a transparent solution was obtained. After this step, 80 mL of prepared solution transferred to 100 mL autoclaves. The fraction was conducted in an electric oven at 100 °C for 12 h. The vessel was cooled to RT and the precipitate was collected by centrifugation and washed with DI water and dried air. The five different powder materials obtained are Z0, Z5, Z7, Z9, Z11 as the names mentioned in Table 2. Finally, these samples were pressed under 4 tons for 5 min into disk shaped compacts with a thickness of 2 mm and a diameter of 5 mm. Finally, the pressed samples were annealed at 750 °C for 2 h in air.

In this work, the samples are used for investigation of XRD, SEM and Vickers hardness measurements. $Zn_{1-x}B_xO$ ($x = 0.00$, 0.05, 0.07, 0.09, 0.11) pellet samples were identified by means of X-ray diffraction (XRD) using Rigaku Multiflex at room temperature with CuKα ($\lambda = 1.5418$ Å). The XRD data were collected over the range $20° < 2\theta < 80°$ in a scan speed of 3°/min and a step increment of 0.02°. The refinement of cell parameters was performed by use of Jana 2006 software [16]. The average crystallite size is estimated from XRD data using Debye-Scherer's formula, $\langle D\rangle = \kappa\lambda/\beta \cos\theta$ where $\langle D\rangle$ is average crystallite size in Å, κ is the shape factor, λ is the wavelength of the X-ray ($\lambda_{Cu\text{-}K\alpha} = 1.5418$ Å) and β is the corrected full width at half maximum (FWHM) and θ is the Bragg angle of diffraction [17]. The surface morphologies of the samples were performed by scanning electron microscopy (SEM) (FEI Quanta Feg 250).

Vickers microhardness measurements of the samples were performed with Vickers microhardness meter (SHIMADZU) at room temperature to study the effect of the additives on the mechanical properties of the samples. The load was applied for 10 s and varied in the range of 0.245–2.940 N. All measurements were averaged by pressing the notch on five different surfaces of the sample so that the marks were not overlapped.

3. Results and discussion

3.1. XRD, SEM and EDS analyses

Fig. 1 shows the XRD patterns of the $Zn_{1-x}B_xO$ nanoparticles with $x = 0.00$, 0.05, 0.07, 0.09, 0.11 boron content. Some of the Miller indices are indicated in Fig. 1. The XRD patterns of all the samples are analyzed with the standard card for bulk ZnO with a hexagonal wurtzite structure (ICDD Card no.36-1451) and all samples crystallize in hexagonal wurtzite structure. It was found that there is no characteristic peaks related to B and impurity phases, that is, the B atom entered into the ZnO crystal structure. Fig. 2 shows the superposition of the experimental and the calculated pattern for each samples. The bottom curve shows the difference between the observed and calculated profiles. The quality factors (R_p, R_{wp}) and the goodness of fit (GOF) values are obtained from the Rietveld analysis [16] of the X-rays data and are listed in Table 1. All characteristic peaks of the ZnO are covered by the calculated curve. The fitting results show that the cell parameters are very close to those reported by many groups for the ZnO samples [4,18–20]. It was observed from the XRD results that crystal structure unchanged but intensity of (100) and (200) changed with the B content. One can see from the figure that the main peaks (100) and (200) intensity of the Z5 sample decreased in comparison with the Z0 sample. The decrease in the peak intensities may point out the decrease in grain growth and orientation in the presence of the B content, leading to the decrease of the microhardness value which is in good agreement with our microhardness measurements. Then, the intensity of the peaks increased with increasing the B concentration, leading to the increase in microhardness values. The decrease of intensity and the increase of full width at half maximum (FWHM) for Z5 sample indicate that crystallite size became smaller when compared with undoped sample Z0.

The average crytallite sizes were evaluated for the main peaks of (101), (002) and (100), and are embedded in Table 1. It was obtained from the table that the crystallite size values decrease with the increase in B amount. This result is consistent with microhardness measurements in the present study.

To investigate the surface morphologies of the samples SEM micrographs are taken and depicted in Fig. 3. The irregular appearance and the size distribution of the particles are observed for all samples. From the SEM images, uniform granularity was

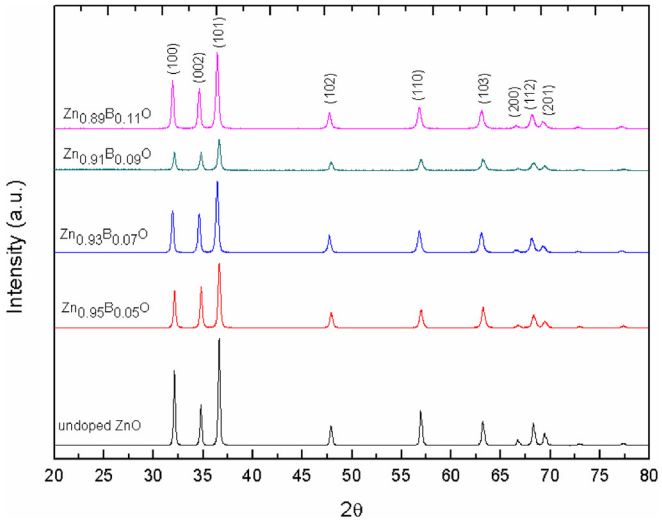

Fig. 1. XRD patterns for undoped and $Zn_{1-x}B_xO$ ($x = 0$, 0.05, 0.07, 0.09, 0.11) nanopowders.

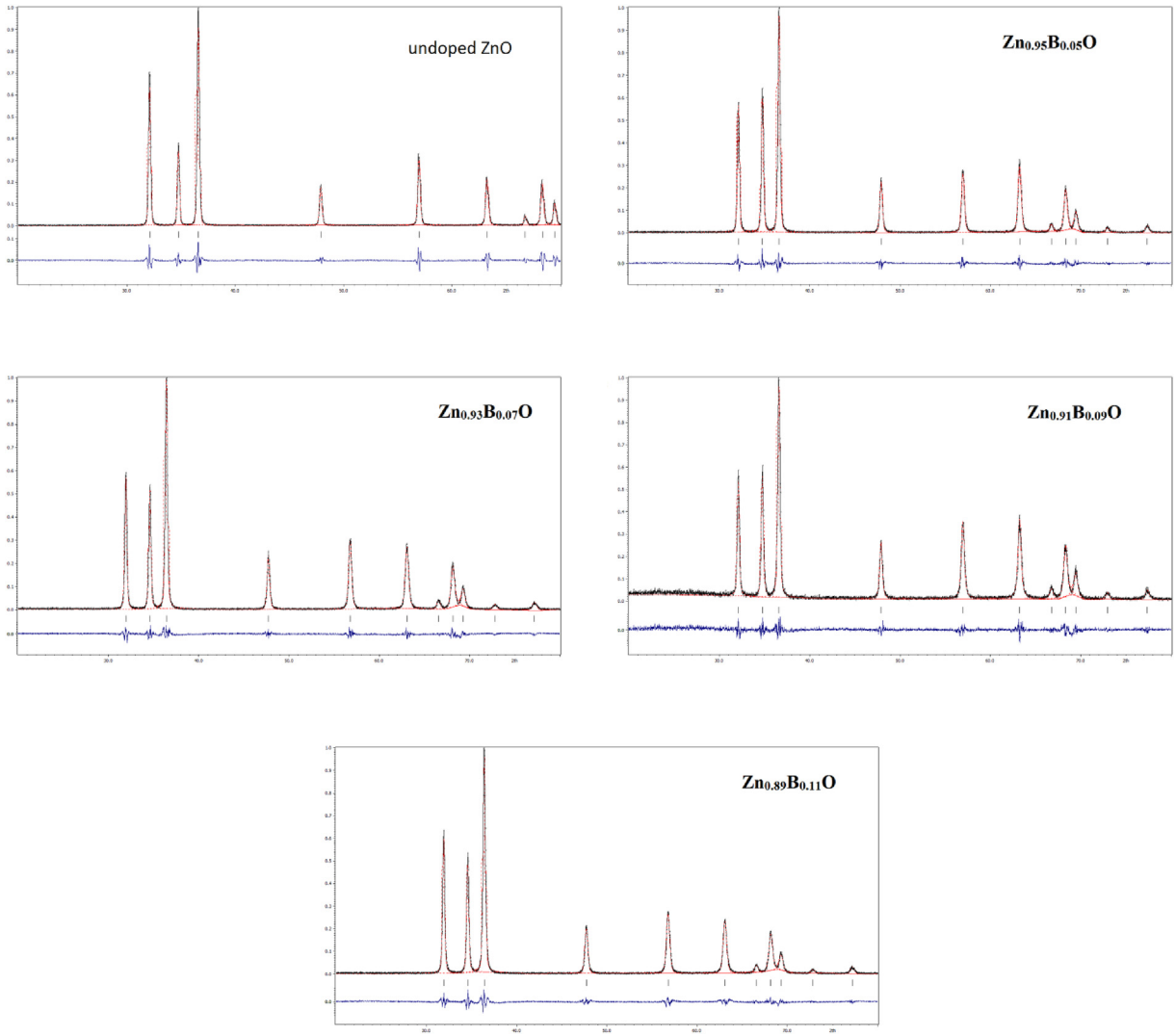

Fig. 2. Jana2006 refinement patterns for undoped ZnO, $Zn_{0.95}B_{0.05}O$, $Zn_{0.93}B_{0.07}O$, $Zn_{0.91}B_{0.09}O$ and $Zn_{0.89}B_{0.11}O$ samples.

Table 1
Details of Jana2006 refinement of undoped ZnO, $Zn_{0.95}B_{0.05}O$, $Zn_{0.93}B_{0.07}O$, $Zn_{0.91}B_{0.09}O$ and $Zn_{0.89}B_{0.11}O$ samples (GOF, RP, RWP, agreement factors).

Samples	Undoped ZnO	$Zn_{0.95}B_{0.05}O$	$Zn_{0.93}B_{0.07}O$	$Zn_{0.91}B_{0.09}O$	$Zn_{0.89}B_{0.11}O$
Symmetry	Hexagonal	Hexagonal	Hexagonal	Hexagonal	Hexagonal
Space Group	$P6_3/mmc$	$P6_3/mmc$	$P6_3/mmc$	$P6_3/mmc$	$P6_3/mmc$
a(Å)	3.2483	3.2483	3.2460	3.2478	3.2463
c(Å)	5.2043	5.2029	5.1995	5.2019	5.1990
α (° degree)	90.000	90.000	90.000	90.000	90.000
β (° degree)	90.000	90.000	90.000	90.000	90.000
δ (° degree)	120.000	120.000	120.000	120.000	120.000
Diffractometer	Rigaku	Rigaku	Rigaku	Rigaku	Rigaku
Radiation type	CuK_α	CuK_α	CuK_α	CuK_α	CuK_α
Monochromator	Graphite	Graphite	Graphite	Graphite	Graphite
Wavelength (Å)	1.5406	1.5406	1.5406	1.5406	1.5406
Refined profile range (2Θ°)	20.00–80.00°	20.00–80.00°	20.00–80.00°	20.00–80.00°	20.00–80.00°
Step size (2Θ°)	0.02	0.02	0.02	0.02	0.02
GOF	3.66	2.78	3.65	2.59	3.26
R_P	12.77	10.17	11.14	13.16	10.31
R_{WP}	20.73	17.80	21.95	18.31	19.06
V	47.6	47.5	47.5	47.5	47.4

observed, grains were brightly visible and the particle boundaries are irregular but almost clear for all the samples. As can be clearly seen from the micrographs, its distribution in the ZnO microstructure becomes denser and more compact as the B concentration increases. This may be related to the reduction in grain size, which was confirmed by the XRD results. Porosity and

Table 2
The average crytallite sizes of the $Zn_{1-x}B_xO$ nanoparticle at different boron concentrations.

Samples	Called as	D (nm)
ZnO	Z0	61.50
$Zn_{0.95}B_{0.05}O$	Z5	36.97
$Zn_{0.93}B_{0.07}O$	Z7	36.65
$Zn_{0.91}B_{0.09}O$	Z9	36.59
$Zn_{0.89}B_{0.11}O$	Z11	34.85

intergranular voids are observed to be more frequent in the Z5 sample, as shown in Fig. 3b. It is concluded that stronger grain connectivity could be obtained with increasing B concentration owing to a reduction in intergranular voids [21]. The denser and more compact structure could be attributed to a harder microstructure. The SEM images reveals that the average grain size significantly depends on the B concentration. The boron atoms act as nucleation centers in the vacancy sites of ZnO. So, B atoms might result in a decrease of the average grain size. Based on the XRD and SEM results, it is expected that the smaller grain size, less number and size of voids, better grain connectivity and denser surface with increasing the B addition would make the hardness value higher which is what we observe and discuss below in Section 3.2. The morphology of ZnO samples enhanced by boron concentration and this enhancement makes the microhardness value increase.

EDS spectra of $Zn_{1-x}B_xO$ nanoparticles are shown in Fig. 4. The EDS experimental results indicate that the B concentration level tends to increase systematically with the increase of dopant level, verifying the introduction of B impurities into the bulk ZnO crystal structures.

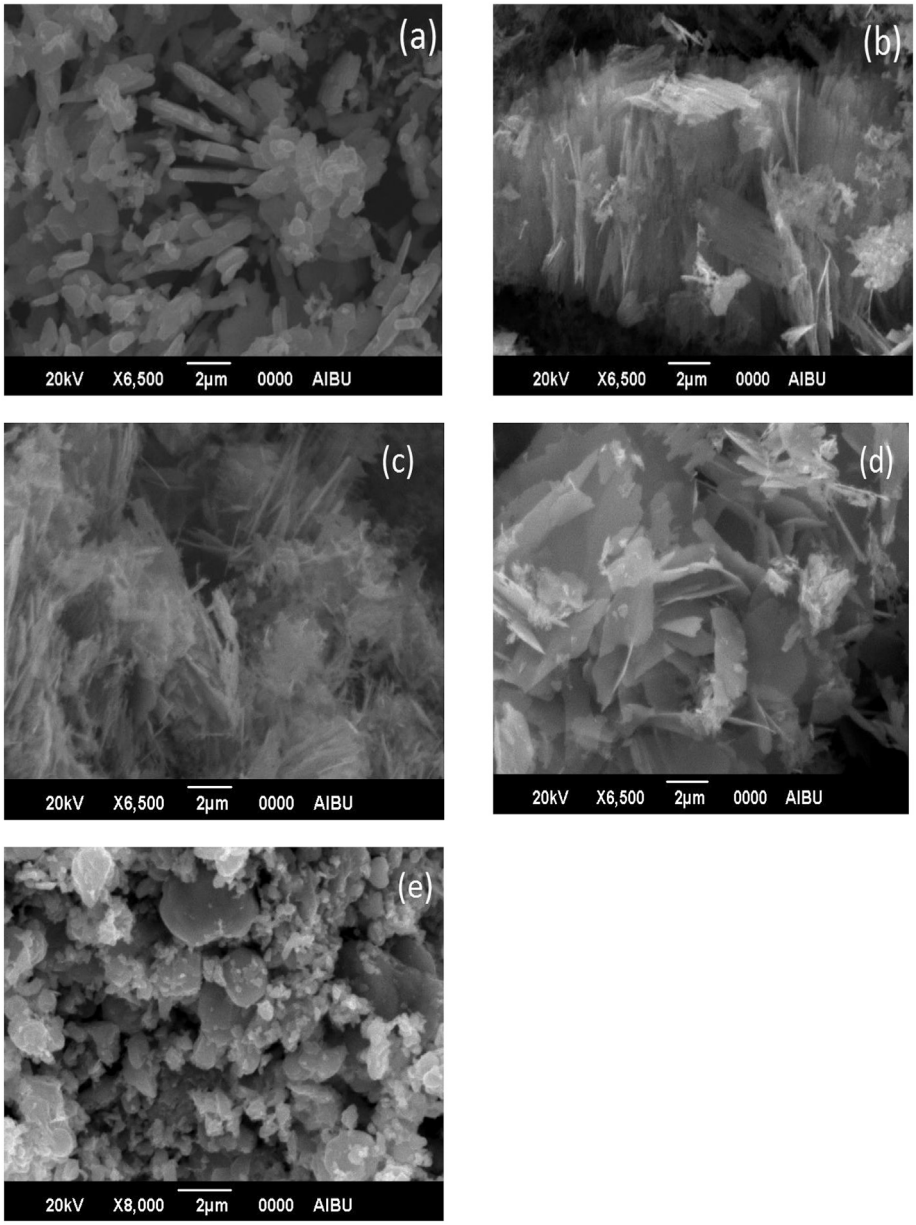

Fig. 3. SEM images of the $Zn_{1-x}B_xO$ powders prepared at different B concentrations (a) undoped (b) 5%, (c) 7%, (d) 9% and (e) 11%.

3.2. Vickers microhardness measurements

The Vickers hardness of the materials can be calculated as

$$H_v = 1854.4\left(P/d^2\right) \quad \text{(GPa)} \tag{1}$$

where Hv is the Vickers hardness in GPa, P is the applied load in N and d is the indentation size in μm. In order to evaluate the Vickers microhardness values of the materials various loads in the range of 0.245, 0.480, 0.980, 1.960 and 2.940 N are applied to each samples. Average value of indentation diagonal lengths are determined by taking five different locations on each specimen the surface. The values of the load-dependent elastic modulus, (E), and yield strength (Y), were calculated for all samples using the following

Undoped ZnO

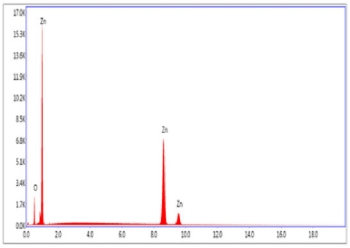

Element	Weight %
O	19.07
Zn	80.93

$Zn_{0.95}B_{0.05}O$

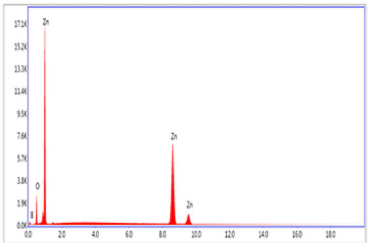

Element	Weight %
B	42.64
O	14.34
Zn	43.02

$Zn_{0.93}B_{0.07}O$

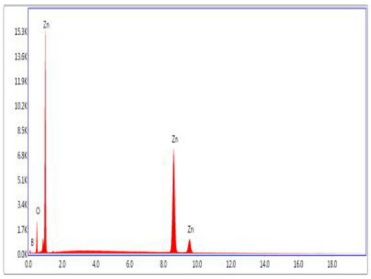

Element	Weight %
B	43.25
O	14.90
Zn	41.85

$Zn_{0.91}B_{0.09}O$

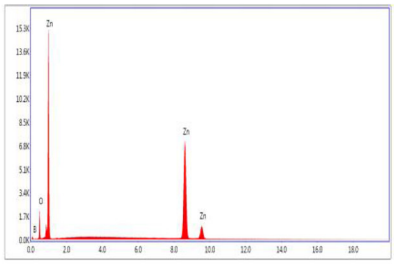

Element	Weight %
B	43.36
O	8.89
Zn	47.75

$Zn_{0.89}B_{0.11}O$

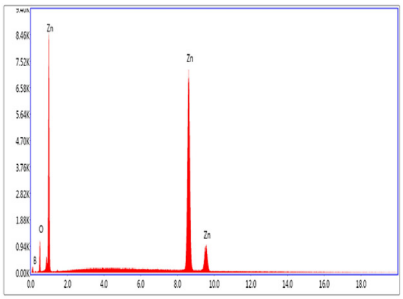

Element	Weight %
B	44.50
O	16.19
Zn	39.31

Fig. 4. SEM attached EDS spectra of undoped ZnO, $Zn_{0.95}B_{0.05}O$, $Zn_{0.93}B_{0.07}O$, $Zn_{0.91}B_{0.09}O$ and $Zn_{0.89}B_{0.11}O$.

formulas, respectively;

$$E = 81.9635H_v \quad (2)$$

$$Y \approx H_v/3 \quad (3)$$

Fracture toughness can be determined from.

$$KIC = c\sqrt{2E|\alpha|} \quad (4)$$

where α is the surface energy, c can be positive or negative value depending on ISE or RISE behavior, respectively. Brittleness (B_i) and ductility (D) parameters for each sample were calculated from the following equations:

$$B_i = H_v/K_{IC} \text{ and } D = 1/B_i \quad (5)$$

The load-dependent H_v, E, Y, K_{IC}, B_i and D values for all the samples are displayed in Table 3. Fig. 5 depictes the applied load dependence of hardness for all the samples. As seen from Fig. 5, the microhardness of the samples decreases with both decreasing the boron amount and applied load and reaches a saturated region at about 1.96 N which indicates that all the samples show RISE behavior. Among the samples, the Z0 sample has the greatest hardness value. Among the B-doped samples, the Z5 sample has the smallest hardness value. The Z5 sample has the larger grain, crystallite sizes and the worser grain connectivity which is in good agreement with the XRD and SEM analyses. One can see from the figure that the microhardness value of the Z5 sample decreased in comparison with the Z0 sample. B addition is found to degrade the hardness of the samples which might be result of either phase segregation due to impurities and/or an increase in voids because of boron incorporation or as it is also observed a changes in the grain boundaries from SEM and XRD data. Then, the value of microhardness increases with the increase in boron content. We have also observed from the XRD and SEM results that the smaller grain size, less number and size of voids, better grain connectivity and denser surface with increasing the B content make the hardness value higher. The morphology of ZnO samples enhanced by boron concentration and this enhancement makes the microhardness value increase.

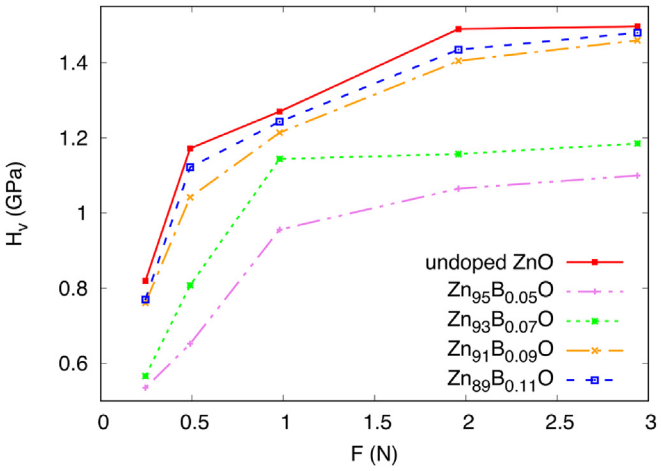

Fig. 5. Variations of microhardness with load for the samples.

In recently, mechanical properties of Al, Mg,Y doped ZnO were investigated [21–24]. It was found that both Al and Mg concentrations decreased the microhardness value in comparision with ZnO [22–24]. In the present study, the value of microhardness of Z5 sample is 0.535 GPa while the value of Al doped ZnO sample is 0.580 GPa at 0.245 N. Kaya et al. found that the microhardness value increased with increasing Yttrium content in ZnO. The value of ZnO was found ton be 0.0253 GPa and the present study value is 1.490 GPa at 2.0 N. This difference can be related to the sample preparation route. The present study sample preparation is hydrothermal method and that of previous study is sol-gel.

Moreover, The *E, Y, K_{IC}, B_i* and *D* values depend on both load and boron content. The behavior of these values has the same as hardness value, that is, these values increased when the applied load and B concentration increased.

Table 3
H_v, E, Y and K_{IC} load-dependent values of the samples.

Samples	*F (N)*	*H_v (GPa)*	*E (GPa)*	*Y (GPa)*	*$K_{IC}(MPa/m^{1/2})$*	*$B_i(m^{-1/2})$*	*$D(m^{1/2})$*
Undoped ZnO	0.245	0.820	67.210	0.273	40.925	20.036	0.049
	0.490	1.172	96.060	0.390	48.926	23.954	0.041
	0.980	1.270	104.090	0.423	50.930	24.936	0.040
	1.960	1.490	122.120	0.496	55.165	27.009	0.037
	2.940	1.497	122.690	0.499	55.294	27.073	0.036
$Zn_{0.95}B_{0.05}O$	0.245	0.535	43.850	0.178	37.306	14.340	0.069
	0.490	0.652	53.440	0.217	41.184	15.831	0.063
	0.980	0.956	78.350	0.318	49.868	19.170	0.052
	1.960	1.065	87.290	0.355	52.636	20.233	0.049
	2.940	1.100	90.16	0.366	53.494	20.563	0.048
$Zn_{0.93}B_{0.07}O$	0.245	0.566	46.390	0.188	35.193	16.082	0.062
	0.490	0.807	66.220	0.269	42.048	19.192	0.052
	0.980	1.144	93.760	0.381	50.033	22.864	0.044
	1.960	1.157	94.830	0.385	50.318	22.993	0.043
	2.940	1.185	97.120	0.395	50.922	23.270	0.042
$Zn_{0.91}B_{0.09}O$	0.245	0.761	62.370	0.253	42.558	17.881	0.055
	0.490	1.042	85.400	0.347	49.799	20.924	0.047
	0.980	1.214	99.500	0.404	53.753	22.584	0.044
	1.960	1.406	115.150	0.468	57.826	24.314	0.041
	2.940	1.460	119.66	0.486	58.948	24.767	0.040
$Zn_{0.89}B_{0.11}O$	0.245	0.770	63.11	0.256	34.900	22.063	0.045
	0.490	1.122	91.96	0.374	42.128	26.633	0.037
	0.980	1.239	101.55	0.413	44.342	27.941	0.035
	1.960	1.435	117.61	0.478	47.643	30.119	0.033
	2.940	1.440	118.02	0.480	47.726	30.172	0.033

3.3. Analyses and modeling

In this section, the load dependent microhardness values of the nanopowder samples were analyzed by using Meyer's law, the proportional sample resistance (PSR), elastic/plastic deformation (EPD), indentation-induced cracking (IIC), and the Hays–Kendall (HK) models [25–27].

3.3.1. Meyer's law

One of the simple methods of defining ISE behavior is the Meyer's Law, which is defined by the following formula.

$$F = Ad^n \tag{6}$$

where n is the Meyer number while A is the hardness constant. If n < 2 (n > 2), material shows the ISE (the RISE) behavior. When n = 2 the hardness is the load independent and gives Kick's Law as follow.

$$F = A_{IK}d^2 \tag{7}$$

The ln d dependence of ln F graphs of the samples are plotted in Fig. 6. Slope of this figure is related to n and the vertical intercept is related to A_{IK}. The obtained n and A_{IK} values are given in Table 4. Meyer's number of all samples are greater than 2 which confirms the RISE behavior.

3.3.2. PSR model

Li and Bradt developed a model which is called PSR to evaluate the true hardness value of materials having ISE behavior [28]. This model is formulated as:

$$\frac{F}{d} = \alpha + \beta d \tag{8}$$

where α and β are apparent and true hardness constants, respectively. α and β are extracted from d dependent F/d graph as shown in Fig. 7. Increasing the range of loads was found to a nonlinear relation between F/d versus d data. The true hardness values are evaluated according to the PSR model as;

$$H_{PSR} = 1854.4\beta \tag{9}$$

The obtained α, β and H_{PSR} values are given in Table 5. It was observed from the table that α values for all samples were negative, confirming that all materials show plastic deformation and the RISE behavior. The β constant decreases with the increasing of boron concentration while the α value is not monotonus for all the samples. These obtained values show that the surface of the material after the identer has been dipped and removed has not been relaxed.

It was observed from the table that the true hardness value increases with increasing the applied load and the B fraction which is consistent with the apparent hardness value for each sample. However, the true hardness according to the PSR model is higher than the saturation value in the plateau region. For the Z0 sample, true hardness according to the PSR model is 1.910 GPa which is higher than the saturation value (H_v = 1.490–1.497 GPa) in the plateau region. All the other samples, also, display the same trend which shows that the hardness values deduced from the PSR model are all greater than the saturation value.

3.3.3. EPD model

In Refs. [29,30], the applied load dependent indentation size for the elastic or plastic deformation model is given by

$$F = A_2(d_p + d_e)^2 \tag{10}$$

where A_2 is a constant and d_p is related to plastic deformation. A_2 and d_e values can be obtained from $F^{1/2}$ versus of d_p graph as displayed in Fig. 8. The true hardness value can be evaluated as;

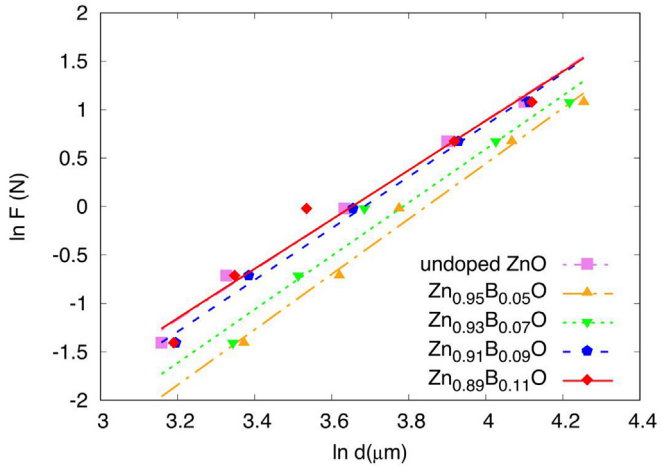

Fig. 6. Variation of applied load ln F with diagonal ln d for the samples.

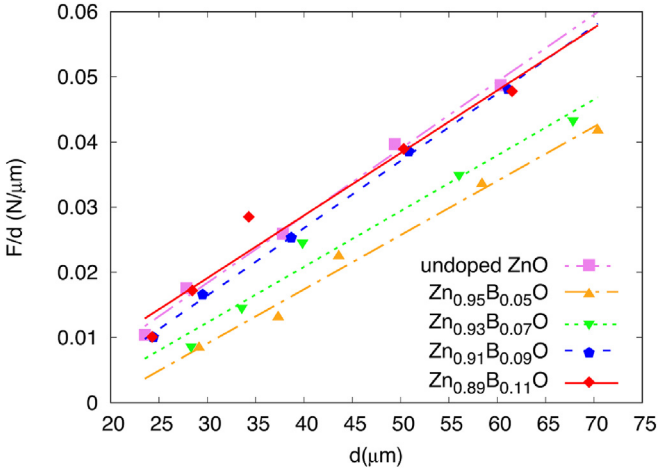

Fig. 7. Plots of F/d versus d for the samples.

Table 4
The extracted and calculated data according to Meyer's Law.

Samples	$\ln A_{IK}$ (N/μm^2)	Meyer member (n)
Undoped ZnO	−9.407	2.574
$Zn_{0.95}B_{0.05}O$	−10.989	2.858
$Zn_{0.93}B_{0.07}O$	−10.447	2.760
$Zn_{0.91}B_{0.09}O$	−9.831	2.668
$Zn_{0.89}B_{0.11}O$	−9.309	2.548

Table 5
The extracted and calculated data according to PSR model.

Samples	α (N/μm)	β (N/μm^2)	H_{PSR}(GPa)	H_v(GPa)in plateu region
Undoped ZnO	−0.01246	0.00103	1.9100	1.490–1.497
$Zn_{0.95}B_{0.05}O$	−0.01587	8.316×10^{-4}	1.5421	0.956–1.100
$Zn_{0.93}B_{0.07}O$	−0.01335	8.551×10^{-4}	1.5856	1.144–1.185
$Zn_{0.91}B_{0.09}O$	−0.01452	8.987×10^{-4}	1.6665	1.214–1.460
$Zn_{0.89}B_{0.11}O$	−0.00965	9.592×10^{-4}	1.7787	1.239–1.440

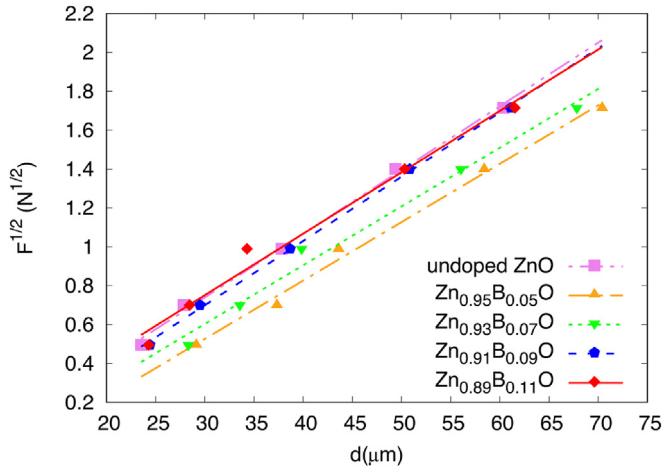

Fig. 8. Plots of diagonal lengths versus the square root of the applied loads for the samples.

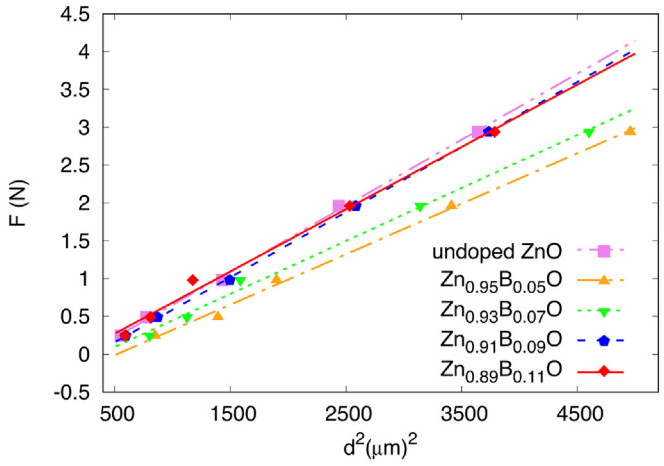

Fig. 9. Graph of the applied load against the square of the diagonal length for the samples.

$$H_{EPD} = 1854.4A_2 \quad (11)$$

From Fig. 8, the $A_2^{1/2}$, d_e and H_{EPD} values are extracted and tabulated in Table 6. As can be seen from Table 6, the d_e values of all the samples are negative which indicates that plastic deformation is observed for all the samples. It was obtained that the extracted true hardness values according to this model are greater than that for apparent hardness and are greater than that of the PSR model.

3.3.4. HK model

Hays and Kendall [31] modified the Kick's law [32] as follows

$$W_{HK} - F = A_{HK}d^2 \quad (12)$$

where A_{HK} is a load-independent constant and W_{HK} is the minimum load to initiate plastic deformation. Fig. 9 exhibits F(N) versus d^2 (μm) graphs for all the samples. The values of A_{HK} and W_{HK} were extracted by fitting our data with this model and tabulated in Table 7. According to this model, the true hardness values are calculated from following relation

$$H_{HK} = 1854.4A_{HK} \quad (13)$$

The calculated hardness H_{HK} (GPa) values are summarized in Table 7. Since the W_{HK} values are negative, it can be said that all the samples show RISE behavior. Again, it was found that the extracted true hardness values according to this model are greater than that for apparent hardness and are lower than that of the PSR and EPD model.

3.3.5. IIC model

Indentation-Induced Cracking (IIC) model is advanced to explain the RISE behavior by proposed Li and Bradt [28]. RISE behavior is based on the following explanations; the applied indentation test load at the point of maximum penetration during the loading half-cycle will be balanced by the total specimen resistance. Therefore,

Table 7
The extracted and calculated data according to HK model.

Samples	A_{HK} (N/(μm)^2)	W_{HK}(N)	H_{HK} (GPa)	H_v(GPa)in plateu region
Undoped ZnO	8.74×10^{-4}	−0.22	1.620	1.490–1.497
$Zn_{0.95}B_{0.05}O$	6.68×10^{-4}	−0.35	1.238	0.956–1.100
$Zn_{0.93}B_{0.07}O$	7.01×10^{-4}	−0.26	1.299	1.144–1.185
$Zn_{0.91}B_{0.09}O$	8.61×10^{-4}	−0.27	1.596	1.214–1.460
$Zn_{0.89}B_{0.11}O$	8.23×10^{-4}	−0.14	1.526	1.239–1.440

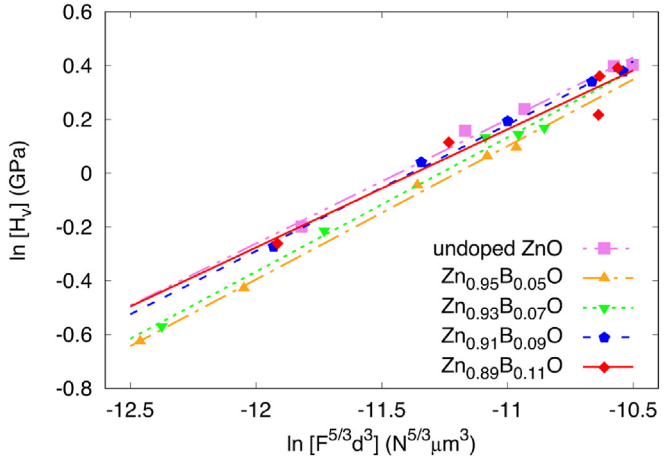

Fig. 10. Variation of $\ln H_v$ versus $\ln (F^{5/3}/d^3)$, according to the IIC model.

Table 6
The extracted and calculated data according to EPD model.

Samples	$A_2^{1/2}$(N$^{1/2}$/μm)	d_e (μm)	H_{EPD} (GPa)	H_v (GPa) in plateu region
Undoped ZnO	0.0328	−0.244	1.995	1.490–1.497
$Zn_{0.95}B_{0.05}O$	0.0300	−0.375	1.668	0.956–1.100
$Zn_{0.93}B_{0.07}O$	0.0302	−0.304	1.691	1.144–1.185
$Zn_{0.91}B_{0.09}O$	0.0330	−0.292	2.019	1.214–1.460
$Zn_{0.89}B_{0.11}O$	0.0316	−0.197	1.851	1.239–1.440

Table 8
The extracted and calculated data according to IIC model.

Samples	m	lnK ($N^{(3-5m)/3}/\mu m^{(2-3m)}$	H_{IIC} (GPa)	H_v(GPa)in plateu region
Undoped ZnO	0.46137	5.2753	1.249	1.490–1.497
$Zn_{0.95}B_{0.05}O$	0.49593	5.5562	0.861	0.956–1.100
$Zn_{0.93}B_{0.07}O$	0.49924	5.6252	0.972	1.144–1.185
$Zn_{0.91}B_{0.09}O$	0.47015	5.3527	1.176	1.214–1.460
$Zn_{0.89}B_{0.11}O$	0.43914	4.9937	1.208	1.239–1.440

Table 9
The results of apparent microhardness at the plateau region and true hardness values extracted by using IIC, HK, EPD and PSR models.

Samples	H_{IIC} (GPa)	H_{HK} (GPa)	H_{EPD} (GPa)	H_{PSR}(GPa)	H_v (GPa) in plateu region
Undoped ZnO	1.249	1.620	1.995	1.910	1.490–1.497
$Zn_{0.95}B_{0.05}O$	0.861	1.238	1.668	1.542	0.956–1.100
$Zn_{0.93}B_{0.07}O$	0.972	1.299	1.691	1.585	1.144–1.185
$Zn_{0.91}B_{0.09}O$	1.176	1.596	2.019	1.666	1.214–1.460
$Zn_{0.89}B_{0.11}O$	1.208	1.526	1.851	1.778	1.239–1.440

the applied load of the indentation can be expressed by four individual space resistances, i.e., the plastic deformation, the elastic deformation, the friction at the indentor/specimen face interface and the specimen cracking resistance. In addition, while cracking is defined as RISE behavior, friction and elastic deformation lead to normal ISE. In this model, Vickers microhardness values were calculated by the diamond indenter as given in Ref. [31].

$$H_{app} = \lambda_1 K_1 \left(\frac{F}{d^2}\right) + K_2 \left(\frac{F^{5/3}}{d^3}\right) \quad (14)$$

where d is the trace's diameter and λ_1, K_1 and K_2 are constants. The K_1 is the geometrical conversion factor whose value depends on the identer while the K_2 is load dependent. $\lambda_1 = 1$ and K_2 $(F^{5/3}/d^3) = 0$ for an ideal plastic materials while $\lambda_1 = 0$ for ideal brittle solids. If the angle of 148° between the opposite edges of the Vickers diamond indenter the indentation diagonal *(d)* should be equal 7 times indentation depth *(h)*. This relation is well compatible for hardness data on semiconductors [15,33–36]. In the case of a perfect brittle material, true hardness can be given by

$$H_{app} = K\left(\frac{P^{5/3}}{d3}\right)^m \quad (15)$$

where m and K are load independent constants. The ln (H_v) versus ln ($F^{5/3}/d^3$) graphs of all the samples are plotted in Fig. 10. Slope of this figure is proportional to m while vertical intercept is proportional to lnK. The obtained m, lnK and true hardness H_{IIC} values are given in Table 8. The exponent m is used to define the ISE or RISE behavior. If m is greater (less) than 0.6, the ISE behavior (RISE behavior) is observed [36,37]. As can be seen from Table 9, the m values of all the samples are less than 0.6 and the RISE behavior is observed for all the samples. As can be seen from the table, there is no trend in m *and* K values for different samples while H_{IIC} of the samples increase with increasing B fraction close to the plateau hardness values.

As a summary of the results presented above, we have used Meyer, PSR, EPD, HK and IIC models to analyze the micro-indentation data in B doped ZnO samples and the resulting micro-hardness data are displayed in Table 9. According to the results, the IIC model is the most appropriate model to address the RISE behavior for the samples in this work.

The RISE behavior generally is due to relative predominance nucleation and multiplication of dislocations. This behavior can also resulting from the relative predominance of the activity of either two sets of slip planes of a particular slip system or two slip systems below and above a particular load [25].

4. Conclusions

In this study, $Zn_{1-x}B_x$ O, (x = 0.00, 0.05, 0.07, 0.09,0.11) nanopowders were prepared by the hydrothermal method. The investigations consist of XRD, SEM and static Vickers hardness measurements. The main findings of the study can be summarized as follows:

1) The XRD results proved that $Zn_{1-x}B_xO$ crystallize in hexagonal wurtzite structure without any impurities and additional phases. In addition, the crystallite size decreases with increasing the B concentration which is consistent with the micro-hardness measurements.
2) From the SEM analysis, we have found that the Z5 sample has smaller grain size, denser surface, better grain connectivity and low void density compared to the Z7, Z9 and Z11 samples. These findings are in agreement with the apparent and true hardness values.
3) B addition is found to degrade the hardness of the samples which might be result of either phase segregation due to an increase in voids because of boron incorporation or as it is, also observed from SEM and XRD data, a changes in the grain boundaries.
4) The micro-hardness values increased with increasing both the applied load and the B content. In our micro-hardness measurements, in contrast to the ISE, a RISE behavior is observed.
5) We have found that the IIC is the most successful model to explain the load versus indentation data of our samples among the five models we have used in the fitting.

Acknowledgements

This research partially supported by Bolu Abant Izzet Baysal University Scientific Research Projects Coordination Department under the Grant No. BAP– 2013.03.02.609. The authors would like to thank to the Kastamonu University Research and Application Center for the supports.

References

[1] U. Ozgur, I.A. Ya, C. Liu, A. Teke, M.A. Reshchikov, S. Doğan, et al., J. Appl. Phys. 98 (2005), 041301.
[2] A. Moezzi, A.M. McDonagh, M.B. Cortie, Chem. Eng. J. 185–186 (2012) 1–22.
[3] S. Baruah, J. Dutta, Hydrothermal growth of ZnO nanostructures, Sci. Technol. Adv. Mater. 10 (2009), 013001.
[4] S.D. Senol, O. Ozturk, C. Terzioğlu, Ceram. Int. 41 (2015) 11194–11201.
[5] Z. Zang, A. Nakamura, J. Temmyo, Optic Express 21 (9) (2013) 11448.
[6] Z. Zang, X. Tang, J. Alloys Compd. 619 (2015) 98–101.
[7] C. Lia, C. Hana, Y. Zhang, Z. Zang, M. Wang, X. Tang, J. Du, Sol. Energy Mater. Sol. Cell. 172 (2017) 341–346.
[8] P. Wang, X. Zhao, B. Li, Optic Express 19 (12) (2013) 11271.
[9] L. Arda, O. Ozturk, E. Asikuzun, S. Ataoglu, Powder Technol. 235 (2013) 479.
[10] E. Asikuzun, O. Ozturk, H.A. Cetinkara, G. Yildirim, A. Varilci, M. Yılmazlar, C. Terzioglu, J. Mater. Sci. Mater. Electron. 23 (2012) 1001.
[11] R. Siddheswaran, R.V. Mangalaraja, Ricardo E. Avilab, D. Manikandan, C. Esther Jeyanthi, S. Ananthakumar, Mater. Sci. Eng. A 558 (2012) 456.
[12] V. Rajkovic, D. Bozic, A. Devecerski, T.M. Jovanovic, Mater. Char. 67 (2012) 129.
[13] S. Zhao, Y. Zhou, Y. Liu, K. Zhao, S. Wang, W. Xiang, Z. Liu, P. Han, Z. Zhang, Z. Chen, H. Lu, K. Jin, B. Cheng, G. Yang, Appl. Surf. Sci. 253 (2006) 726.
[14] R.L. Smith, G. E Sandland, Proc. Inst. Mech. Eng. Vol.I (1922) 623–641.
[15] K. Sangwall, B. Surowska, P. Blaziak, Mater. Chem. Phys. 77 (2002) 511.
[16] V. Petricek, M. Dusek, L. Palatinus, JANA2006, the crystallographic computing system. Institute of Physics, Praha, Czech Republic, in: V. Petricek, M. Dusek, L. Palatinus (Eds.), Z. Kristallogr. 229 (5) (2014) 345.
[17] A. Taylor, X-ray Metallography/A. Taylor, John Wiley & Sons, New York, 1961.
[18] A. Chanda, S. Gupta, M. Vasubdhara, S.R. Joshi, G.R. Mutta, J. Singh, RSC Adv. 7 (2017) 50527–50536.
[19] A.P. Hynes, R.H. Doremus, R.W. Siegel, J. Am. Cream. Soc. 85 (8) (2002) 1979–1987.
[20] M. Shatnawi, A.M. Alsmadi, I. Bsoul, B. Salameh, et al., J. Alloys Compd. 655 (2016) 244–252.
[21] S. Kaya, D. Akcan, O. Ozturk, L. Arda, Ceram. Int. 44 (9) (2018) 10306–10314.
[22] E. Asikuzun, A. Donmez, L. Arda, O. Cakiroglu, O. Ozturk, D. Akcan, M. Tosun, S. Ataoglu, C. Terzioglu, Ceram. Int. 41 (2015) 6326–6334.
[23] M. Tosun, S. Ataoglu, L. Arda, O. Ozturk, E. Asikuzun, D. Akcan, O. Cakiroglu, Mater. Sci. Eng. A 590 (2014) 416–422.
[24] E. Asikuzun, O. Ozturk L. Arda, D. Akcan, S.D. Senol, C. Terzioglu, J. Mater. Sci. Mater. Electron. 26 (10) (2015) 8147–8159.
[25] K. Sangwal, Mater. Chem. Phys. 63 (2000) 145–152.
[26] J. Gong, J. Wu, Z. Guan, J. Eur. Ceram. Soc. 19 (1999) 2625–2631.
[27] E. Asikuzun, O. Ozturk, Ceram. Int. 45 (2019) 4176–4183.
[28] H. Li, R.C. Bradt, J. Mater. Sci. 28 (1993) 917–926.
[29] G.P. Upit, S.A. Varchenya, Phys. Status Solidi (b) 17 (2) (1966) 831–835.
[30] S.J. Bull, T.F. Page, E.H. Yoffe, Phil. Mag. Lett. 59 (1989) 281–288.
[31] C. Hays, E.G. Kendall, Metallography 6 (4) (1973) 275–282.
[32] F. Kick, Das Gesetz der Proportionalen Widerstände and Seine Anwendung, Leipzig Felix Edition, 1885.
[33] K. Sangwal, Cryst. Res. Technol. 44 (10) (2009) 1019–1037.
[34] K. Sangwal, B. Surowska, Mater. Res. Innov. 7 (2003) 91.
[35] H. Li, R.C. Bradt, J. Mater. Sci. 31 (1996) 1065.
[36] S.J. Bull, T.F. Page, E.H. Yoffe, Phil. Mag. Lett. 59 (1989) 281–288.
[37] R. Awad, A.I. Abou Aly, M. Kamal, M. Anas, J. Supercond. Nov. Magnetism 24 (6) (2011) 1947–1956.